ELSEVIER

Agricultural and Forest Meteorology 80 (1996) 87–109

AGRICULTURAL AND FOREST METEOROLOGY

Combining the Penman–Monteith equation with measurements of surface temperature and reflectance to estimate evaporation rates of semiarid grassland

M.S. Moran [a,*], A.F. Rahman [b], J.C. Washburne [c], D.C. Goodrich [d], M.A. Weltz [d], W.P. Kustas [e]

[a] *USDA – ARS US Water Conservation Laboratory, Phoenix, AZ, USA*
[b] *University of Arizona, Department of Soil and Water Science, Tucson, AZ, USA*
[c] *University of Arizona, Department of Hydrology and Water Resources, Tucson, AZ, USA*
[d] *USDA – ARS Southwest Watershed Research Center, Tucson, AZ, USA*
[e] *USDA – ARS Hydrology Laboratory, Beltsville, MD, USA*

Received 25 July 1995; accepted 26 July 1995

Abstract

The Penman–Monteith equation is useful for computing evaporation rates of uniform surfaces, such as dense vegetation or bare soil. This equation becomes less useful for evaluation of evaporation rates at the regional scale, where surfaces are generally characterized by a patchy combination of vegetation and soil. This is particularly true in the arid and semi-arid regions of the world. The approach proposed here is an attempt to use remotely-sensed measurements of surface reflectance and temperature to allow application of the Penman–Monteith theory to partially-vegetated fields without a-priori knowledge of the percent vegetation cover and canopy resistance. Basically, the Penman–Monteith equation was combined with the energy balance equation to estimate the surface temperature (T_s) associated with four states: surfaces characterized by full-cover vegetation and bare soil with evaporation rates at potential and zero. Then, linear interpolations between T_s values computed for full-cover and bare soil conditions were used to provide information at intermediate states based on measurements of actual surface reflectance and temperature. The approach was first tested using ground-based measurements of surface reflectance and temperature at a rangeland site; the results compared well with on-site measure-

* Corresponding author.

SSDI 0168-1923(95)02292-9

ments of surface evaporation rate (RMSE = 29 W m^{-2}). Then, the approach was tested based on a set of four Landsat Thematic Mapper (TM) images acquired in southeast Arizona during 1992. Maps of surface air temperature and wind speed were combined with maps of surface temperature and spectral vegetation index to produce regional estimates of evaporation rates for the grassland biome.

1. Introduction

The Penman–Monteith (P–M) equation is well-known for estimation of evaporation (E) and transpiration (Γ) rates from 'uniform' surfaces (Monteith, 1973; Allen, 1986). It requires knowledge of basic meteorological conditions such as vapor pressure deficit (VPD), air temperature (T_a) and wind speed (U), and estimates of canopy and aerodynamic resistances. The difficulty in measuring the latter two inputs for partially-vegetated sites generally limits application of the P–M equation to full-cover vegetation and bare soil. In fact, the most common application of the P–M equation is for estimation of potential Γ or E from full-cover vegetation or open-water surfaces. Unfortunately, for most resource monitoring/management applications, a value of actual evapotranspiration ($E\Gamma$) rate is far more useful. Actual $E\Gamma$ has been used as a direct indicator of soil moisture content, soil water matrix potential, soil salinity, soil waterlogging, plant water potential, leaf diffusion resistance and photosynthesis, and even final crop yield.

In recent years, there has been a great deal of study to use remotely sensed data to estimate actual $E\Gamma$. One avenue that has proven particularly successful has been the incorporation of remotely sensed spectral measurements with ground-based meteorological measurements in the P–M equation. The link between the P–M equation and remotely sensed measurements of surface temperature was first made by Jackson et al. (1981). They combined the P–M equation with a one-dimensional energy balance equation to allow estimation of the maximum and minimum foliage temperatures (T_{cx}, T_{cm}, where subscript 'c' refers to canopy foliage temperature and subscripts 'x' and 'm' refer to maximum and minimum temperatures, respectively) associated with instantaneous minimum and maximum transpiration rates, respectively. Then, by comparison of these extreme foliage temperatures with a measurement of actual foliage temperature, it was possible to estimate the ratio of actual to potential $E\Gamma$ and infer plant water stress. Based on this theory, they developed the Crop Water Stress Index (CWSI) which has since been used extensively for such important farm applications as irrigation scheduling, predicting crop yields, and detecting certain plant diseases. Because CWSI requires a measurement of foliage temperature and because most airborne and satellite-based sensors measure composite surface temperature (T_s: a composite of soil and vegetation temperatures), application has generally been limited to fully-vegetated sites, such as agricultural fields.

Moran et al. (1994a) suggested that CWSI could be refined for application to partially-vegetated surfaces by including measurements of surface reflectance in addition to surface temperature. Based on the P–M equation, they computed the maximum and minimum soil temperatures (T_{ox}, T_{om}, where subscript 'o' refers to soil temperature) associated with minimum and maximum evaporation rates, respectively. These four

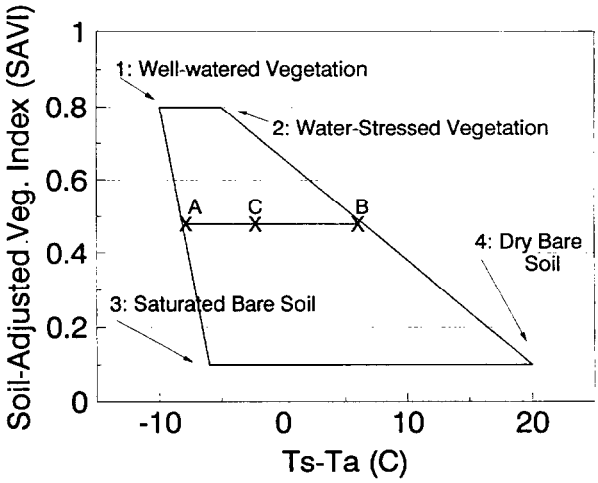

Fig. 1. The hypothetical trapezoidal shape that would result from the relation between $(T_s - T_a)$ and the soil adjusted vegetation index (ranging from ~0.1 for bare soil and ~0.8 for full-cover vegetation). With a measurement of $(T_s - T_a)$ at point C, it would be possible to equate the ratio of actual to potential $E\Gamma$ with the ratio of distances CB and AB.

temperatures (T_{cx}, T_{cm}, T_{ox}, T_{om}) [1] were plotted against a spectral vegetation index (which is linearly correlated with percent vegetation cover; see Huete and Jackson, 1988; Huete, 1988; Moran et al., 1994b) to form a trapezoidal shape that encompassed all possible values of surface temperature for both full-cover and partially-vegetated surfaces (Fig. 1). With a measurement of T_s at point C, it was possible to equate the ratio of actual to potential evapotranspiration with the ratio of distances CB and AB. They defined this ratio as the Water Deficit Index (WDI).

Moran et al. (1994a) gave a theoretical justification (with assumptions and limitations) and experimental demonstration of the WDI for agricultural applications at the field scale. The work presented here is an attempt to apply this theory to semiarid grassland vegetation at the local and regional scale. The goal was to test this operational technique for monitoring changes in surface conditions for applications in regional resource management. As such, we used data from existing meteorological stations and the currently-orbiting Landsat Thematic Mapper (TM). At the local scale, modeled evaporation rates were compared with ground-based measurements at one site; at the regional scale, the modeled evaporation rates for the entire grassland biome were validated with knowledge of recent rainfall events and on-site meteorological conditions. The potential for use in other biomes was also demonstrated.

[1] It is important at this point to emphasize the differences between T_c, T_o and T_s. T_c is the foliage or 'crop' temperature. T_o is the temperature of the soil surface. T_s is the surface composite temperature; that is, a weighted average of soil and vegetation temperatures. When the surface is completely covered by vegetation, then $T_s = T_c$; and when the surface is bare soil, then $T_s = T_o$. Throughout this discussion, all temperatures are assumed to be kinetic values; that is, all radiometric temperature measurements have been corrected for surface emissivity.

2. Background

In numerous studies, the observed negative correlation between surface temperature and spectral vegetation indices (such as Normalized Difference VI (NDVI) and Soil-Adjusted VI (SAVI)) has been related to plant transpiration and soil evaporation. That is, differences in the amount of vegetation, the leaf transpiration rate, and the soil evaporation rate result in variability in surface temperature measurements due to evaporative cooling. For dense vegetation with a complete canopy, the slope of the T_s/NDVI relation has been related to canopy resistance (Sellers, 1987; Hope, 1988; Nemani and Running, 1989). For land surfaces with fractional vegetation cover, Nemani et al. (1993) found that the slope of the T_s/NDVI relation was negatively correlated to a crop-moisture index. These relations have been corroborated by other empirical studies using a variety of sensors at different locations (Goward and Hope, 1989; Hope and McDowell, 1992). Though empirical relations such as these are useful for many applications, they require that the image cover the entire range of vegetation cover to supply sufficient information for computation of the T_s/NDVI slope from the data. Furthermore, they do not work well when the soil moisture of partially-vegetated surfaces is spatially variable within the image, causing considerable scatter in the T_s/NDVI relation. In response to these problems, attempts have been made to incorporate meteorological models with observations of T_s and NDVI to improve estimates of surface conditions over partially-vegetated sites.

Price (1990) used energy balance theory to map regional evaporation rates. He estimated evaporation rates directly from the spatial variations in satellite-derived surface temperature and NDVI. Similarly, Carlson et al. (1990) and Carlson et al. (1994) combined a boundary layer model with vegetation and substrate components with T_s and NDVI measurements to map soil moisture in the surface and root zone over patchy vegetation. Though this was an improvement over strictly empirical approaches, the model still required knowledge of the slope of the T_s/NDVI relation derived from the image data. In refinement of this approach, Gillies et al. (1995) used a Soil-Atmosphere-Vegetation (SVAT) model to produce isolines of T_s/NDVI data corresponding to a variety of surface moisture availability values. These lines were shifted to fit the range of data in the T_s/NDVI scattergram, preserving the basic shape and non-linear spacing. Then, the new isolines were used to convert the T_s/NDVI data to soil moisture availability values and the SVAT model was again run for each pixel value to map evaporation rates. Though this circumvented the need to derive the slope of the T_s/NDVI relation, it was still dependent upon the scatter of the image data. As in the work of Price (1990), the methods of Carlson et al. (1990), Carlson et al. (1994) and Gillies et al. (1995) required spatial variability in the satellite data and did not apply in uniform areas.

Friedl and Davis (1994) used a soil-canopy-sensor (SCS) model and data from the First ISLSCP Field Experiment (FIFE) to conduct a comprehensive study of the land surface properties and processes that produce the distinctive relation between T_s and NDVI. This work was conducted with the hope of exploiting this relation in strategies to model land surface energy balance from satellites. They reported that the observed covariance between T_s and NDVI was due to temperature differences between the soil

and vegetation and variations in fractional vegetation cover. Furthermore, they found the T_s/NDVI relation to be highly date and time specific, and dependent on land cover class. Based on these findings, they suggested that future work should be directed toward incorporating information on soil moisture in invertible surface energy balance models for regional applications.

The approach proposed by Moran et al. (1994a) addresses some of the issues identified by Friedl and Davis (1994). The technique utilized the P–M equation to define the theoretical boundaries of the $T_s - T_a$/SAVI relation based on date- and time-specific meteorological data, and reasonable values of vegetation and soil characteristics. Information about $E\Gamma$ rates was derived from the location of the $T_s - T_a$ and SAVI measurements within the date- and time-specific trapezoid (Fig. 1). This avoided the reliance on empirical interpretation of the T_s/SAVI image scatter, and allowed application of the method to both heterogeneous and uniform areas, regardless of date and time. Moran et al. (1994a) limited their application to irrigated agricultural fields, with emphasis on applications in irrigation scheduling. Thus, it was unclear if the underlying assumptions and inputs were suitable for other important land cover classes, such as rangeland. This issue is the topic of the experiment and analysis presented here.

3. Theory

Jackson et al. (1981) combined the P–M equation with a one-dimensional energy balance equation to derive a computation for foliage-air temperature,

$$(T_c - T_a) = \left[r_a(R_n - G)/C_v\right]\left[\gamma\left(1 + \frac{r_c}{r_a}\right)\Big/\left\{\Delta + \gamma\left(1 + \frac{r_c}{r_a}\right)\right\}\right] - \left[\mathrm{VPD}\Big/\left\{\Delta + \gamma\left(1 + \frac{r_c}{r_a}\right)\right\}\right], \quad (1)$$

where T_c is the crop foliage temperature (°C), T_a the air temperature (°C), r_a the aerodynamic resistance ($s\,m^{-1}$), R_n the net radiant heat flux density ($W\,m^{-2}$), G the soil heat flux density ($W\,m^{-2}$), C_v the volumetric heat capacity of air ($J\,°C^{-1}\,m^{-3}$), r_c the canopy resistance ($s\,m^{-1}$) to vapor transport, γ the psychrometric constant ($Pa\,°C^{-1}$), Δ the slope of the saturated vapor pressure-temperature relation ($Pa\,°C^{-1}$), and VPD the vapor pressure deficit of the air (Pa). Eq. (1) was then solved for the ratio r_c/r_a which was used in the relation

$$\mathrm{CWSI} = 1 - \frac{\Gamma}{E\Gamma_p} = \left[\gamma\left(1 + \frac{r_c}{r_a}\right) - \gamma^*\right]\Big/\left[\Delta + \gamma\left(1 + \frac{r_c}{r_a}\right)\right], \quad (2)$$

where

$$\frac{r_c}{r_a} = \frac{\left[\gamma r_a R_n/C_v\right] - \left[(T_c - T_a)(\Delta + \gamma)\right] - \mathrm{VPD}}{\gamma\left[(T_c - T_a) - r_a(R_n - G)/C_v\right]}, \quad (3)$$

to obtain the ratio of transpiration Γ to potential evapotranspiration $E\Gamma_p$.

Moran et al. (1994a) further developed this work to develop a new concept [termed Vegetation Index/Temperature (VIT) Trapezoid] which combined a spectral vegetation index with surface temperature measurements (a composite of both the soil and plant temperatures) to determine field water deficit conditions for partial cover crops. The spectral vegetation index used in this analysis was the Soil-Adjusted Vegetation Index (SAVI), where

$$\mathrm{SAVI} = (\rho_{\mathrm{NIR}} - \rho_{\mathrm{red}})/(\rho_{\mathrm{NIR}} + \rho_{\mathrm{red}} + L)(1 + L), \tag{4}$$

and ρ_{NIR} and ρ_{red} are the near-IR and red reflectances, respectively, and L is assumed to be 0.5 for a wide variety of leaf area index (LAI) values (Huete, 1988).

Eq. (1) was used to define the four vertices of a trapezoidal shape in a plot of surface-air temperature ($T_s - T_a$) versus SAVI that encompassed all possible combinations of SAVI and $T_s - T_a$ for one vegetation type on one day. That is, for full-cover, well-watered vegetation,

$$(T_s - T_a)_1 = [r_a(R_n - G)/C_v]\left[\gamma(1 + r_{cp}/r_a)/\{\Delta + \gamma(1 + r_{cp}/r_a)\}\right] - \left[\mathrm{VPD}/\{\Delta + \gamma(1 + r_{cp}/r_a)\}\right], \tag{5}$$

where r_{cp} is the canopy resistance at potential evapotranspiration and the subscript 'n' of $(T_s - T_a)_n$ refers to vertex n in Fig. 1. For full-cover vegetation with no available water,

$$(T_s - T_a)_2 = [r_a(R_n - G)/C_v]\left[\gamma(1 + r_{cx}/r_a)/\{\Delta + \gamma(1 + r_{cx}/r_a)\}\right] - \left[\mathrm{VPD}/\{\Delta + \gamma(1 + r_{cx}/r_a)\}\right], \tag{6}$$

where r_{cx} is the canopy resistance associated with nearly complete stomatal closure. For saturated bare soil, where $r_c = 0$ (the case of a free water surface),

$$(T_s - T_a)_3 = [r_a(R_n - G)/C_v]\left[\gamma/(\Delta + \gamma)\right] - \left[\mathrm{VPD}/(\Delta + \gamma)\right], \tag{7}$$

and for dry bare soil, where $r_c = \infty$ (analogous to complete stomatal closure),

$$(T_s - T_a)_4 = [r_a(R_n - G)/C_v]. \tag{8}$$

Monteith (1973) suggested the values of r_{cp} and r_{cx} could be obtained from measurements of stomatal resistance (r_s) and LAI, where

$$r_{cp} = r_{sp}/\mathrm{LAI} \text{ and } r_{cx} = r_{sx}/\mathrm{LAI}, \tag{9}$$

where LAI > 0. Values of minimum and maximum stomatal resistance (r_{sp} and r_{sx}, respectively) are published for many plant types under a variety of atmospheric conditions. If values are not available, reasonable values of $r_{sp} = 25$–$100\ \mathrm{s\,m^{-1}}$ and $r_{sx} = 1000$–$1500\ \mathrm{s\,m^{-1}}$ won't result in appreciable error.

The assumptions associated with the VIT Trapezoid warrant some discussion. First, the VIT Trapezoid is based on the premise that measurements of vegetation cover (V_c) are linearly related to SAVI. Second, one must assume that $T_s - T_a$ is a linear function of V_c, canopy-air temperature ($T_c - T_a$) and soil-air temperature ($T_o - T_a$), where

$$T_s - T_a = V_c(T_c - T_a) + (1 - V_c)(T_o - T_a). \tag{10}$$

This assumption allows straight lines to be drawn between points 2 and 4 and between points 1 and 3 in Fig. 1. A third assumption that links the VIT Trapezoid to crop water conditions is that, for a given R_n, VPD and r_a, variations in $T_c - T_a$ and $T_o - T_a$ are linearly associated with variations in evaporation (E) and transpiration (Γ). That is,

$$T_c - T_a = a + b(\Gamma) \tag{11}$$

and

$$T_o - T_a = a' + b'(E), \tag{12}$$

where a, a', b and b' are semi-empirical coefficients. The above-mentioned assumptions were thoroughly addressed and justified by Moran et al. (1994a).

The relations presented in Eqs. (5)–(12) imply that variations in $T_s - T_a$ are associated with variations in evapotranspiration ($E\Gamma$). Thus, it follows that for a partially-vegetated surface,

$$\mathrm{WDI} = 1 - \frac{E\Gamma}{E\Gamma_p} = \left[(T_s - T_a)_m - (T_s - T_a)_r\right] / \left[(T_s - T_a)_m - (T_s - T_a)_x\right], \tag{13}$$

where WDI is the Water Deficit Index, $E\Gamma$ is the evapotranspiration rate of the surface, $E\Gamma_p$ is the potential evapotranspiration rate, and the subscripts 'm', 'x' and 'r' refer to the minimum, maximum and measured values, respectively. Graphically, WDI is equal to the ratio of distances AC/AB in Fig. 1. Thus, WDI = 0.0 for well-watered conditions and WDI = 1.0 for maximum stress conditions.

4. Experimental data

To test the WDI theory for regional application, data from an experiment, referred to as WG'92, was analyzed for a semiarid region in southeastern Arizona. The experimental site was chosen to encompass the USDA–ARS Walnut Gulch (WG) Experimental Watershed, which has been the location of prior hydrologic remote sensing experiments (Kustas and Goodrich, 1994) and contains extensive hydrologic instrumentation (Renard et al., 1993). WG'92 was conducted during the dry, early-monsoon, mid-monsoon, post-monsoon and 'drying' seasons (from April through November 1992). The experiment was designed to acquire remotely sensed data in the visible, near-infrared (NIR), thermal and microwave wavelengths from a variety of ground, aircraft and satellite platforms, with concurrent measurements of soil moisture, vegetation growth, and energy and water fluxes (summarized in Table 1).

Most ground- and aircraft-based measurements were limited to one site within WG, where a Metflux (MF) station was located with instrumentation for measuring both general meteorological conditions and estimating the surface energy fluxes. This site was in a hilly, grass-dominated subwatershed and was called the Kendall subwatershed.

The WG'92 experiment provided data at two scales for use in this analysis. First, the theory was tested at the local scale with ground-based radiometers acquired at the grass-dominated Kendall site. At this scale, it was possible to compare the results directly with conventional measurements of EΓ rates on site. Then, the technique was

Table 1
Summary of data acquisition and on-site field measurements during the WG'92 experiment

DOY	Date	Weather	TM	ERS-1	VS	OD	RP	SM	STR
114	23 April	Marginal	yes	25 April	21–23 April	yes	yes	yes	G
130	9 May	Clear		14 May		yes	yes	yes	G
146	25 May	Cloudy			27–28 May		yes	yes	G
162	10 June	Clear	yes	18 June		yes	yes	yes	G
178	26 June	Clear	yes		22–23 June		yes	yes	G
194	12 July	Clear	yes		14–15 July	yes			G
210	28 July	Cloudy			28 July		yes	yes	G and A
224	11 August	Clear			11–12 August	yes			G
226	13 August	Marginal	yes		13 August	yes	yes	yes	G
242	29 August	Cloudy		27 August			yes		
250	6 September	Clear				yes			G and A
251	7 September	Clear				yes			G and A
258	14 September	Cloudy			15–16 September			yes	A
274	30 September	Clear	yes	1 October	30 September	yes	yes	yes	G and A
290	16 October	Clear		16 October	16–17 October	yes	yes	yes	G and A
306	1 November	Clear	yes			yes	yes	yes	G and A
322	17 November	Clear	yes		18–20 November	yes	yes	yes	G and A

DOY = day of year 1992, TM = Landsat Thematic Mapper, ERS-1 = ERS-1 Synthetic Aperture Radar, OD = atmospheric optical depth, RP = radiosonde atmospheric profile, VS = vegetation survey measurements at 2–6 sites, SM = gravimetric soil moisture at 4–5 sites, STR = ground (G) and aircraft-based (A) measurements of surface temperature and reflectance.

demonstrated for all grasslands within the region using Landsat Thematic Mapper (TM) data, which covered the southeast corner of Arizona and included 10 distinct vegetation biomes (Fig. 2(a)). The next subsections address the instrumentation and data processing that were the basis for the subsequent analysis.

4.1. Biome designation

A land cover map for this region was extracted from the *Prototype 1990 Conterminous US Land Cover Characteristics Data Set CD-ROM* (Loveland et al., 1991). Thirty-six land cover classes were identified for south-east Arizona and these were merged to form ten associations that were characteristics of this area: agriculture, sage-oak, desert grassland, conifer forest, oak-grassland, sage-creosote, creosote-mesquite, sage-grassland, alpine forest and playa. The playa 'association' is actually a large, dry, barren lakebed located in the northern part of the TM scene.

4.2. Meteorological-energy flux (Metflux)

The Metflux station at Kendall provided local-scale measurements of net radiation, air temperature, surface temperature, wind speed and direction, relative humidity, solar radiation, photosynthetically active radiation (PAR), soil heat flux, soil moisture and soil temperature. The energy balance was determined by taking measurements of net radiation (R_n), soil heat flux density (G), and the temporal variance of air temperature,

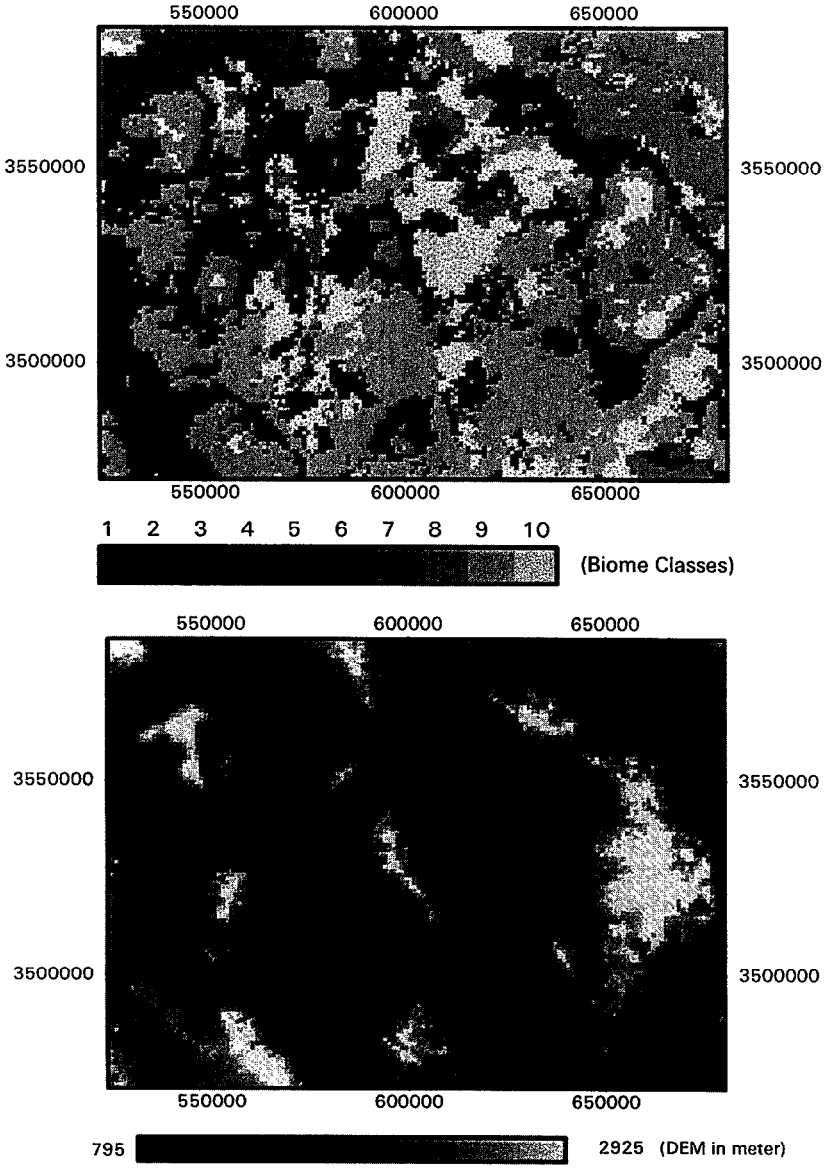

Fig. 2. Images of the study region depicting (a) vegetation biomes [1: agriculture, 2: sage-oak, 3: grassland, 4: conifer, 5: oak-grass, 6: sage-creosote, 7: creosote-mesquite, 8: sage-grass, 9: alpine, and 10: Wilcox Playa] and (b) elevation [with symbols designating Ft. Huachuca (airstrip), Tombstone (box grid), Kendall (circle) and Lucky Hills (windmill)]. Images from DOY 162 depicting, (c) air temperature, (d) wind speed, (e) surface temperature and (f) SAVI.

which was used in computing sensible heat flux density (H) and solving for latent heat flux density (LE) as a residual, i.e., $LE = -(R_n - G - H)$. The instrumentation and theoretical foundation for these stations were described in detail by Kustas et al. (1994). They found that the LE values obtained with this instrumentation were within 20% of

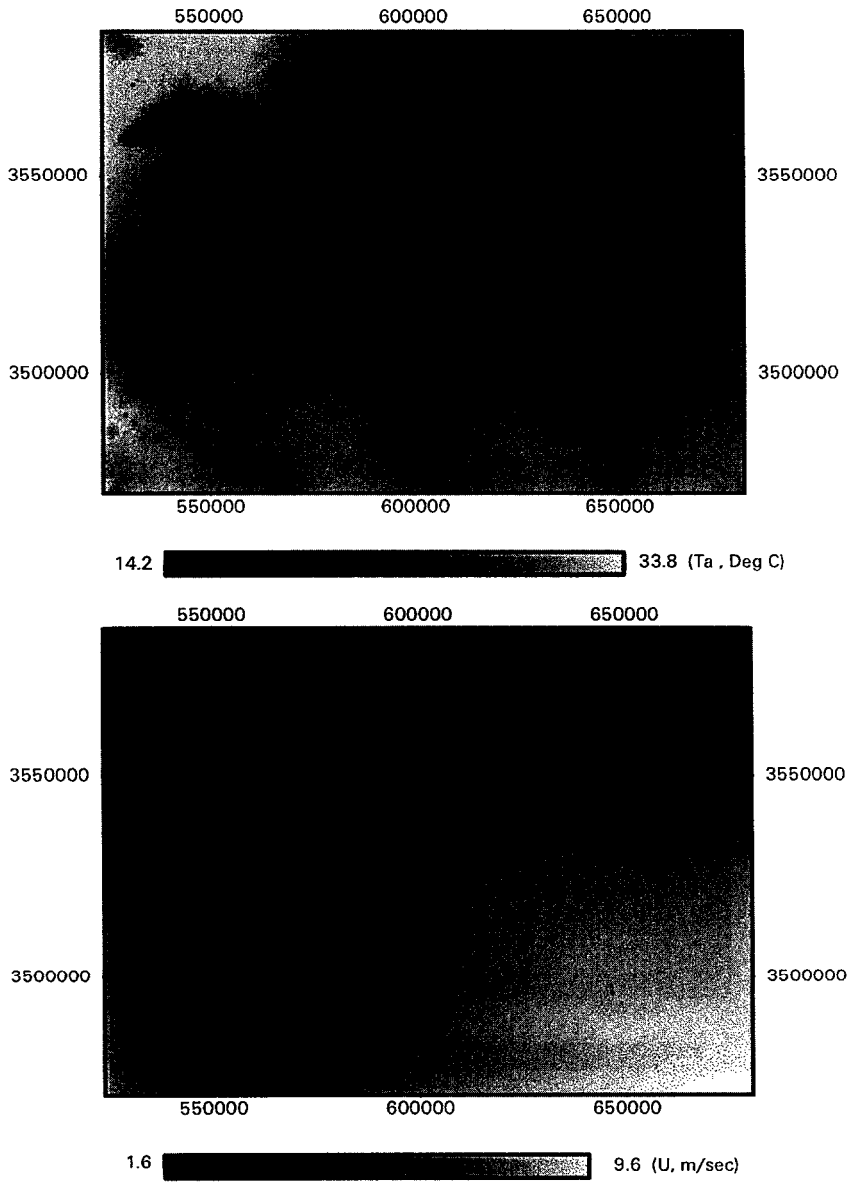

Fig. 2 (continued).

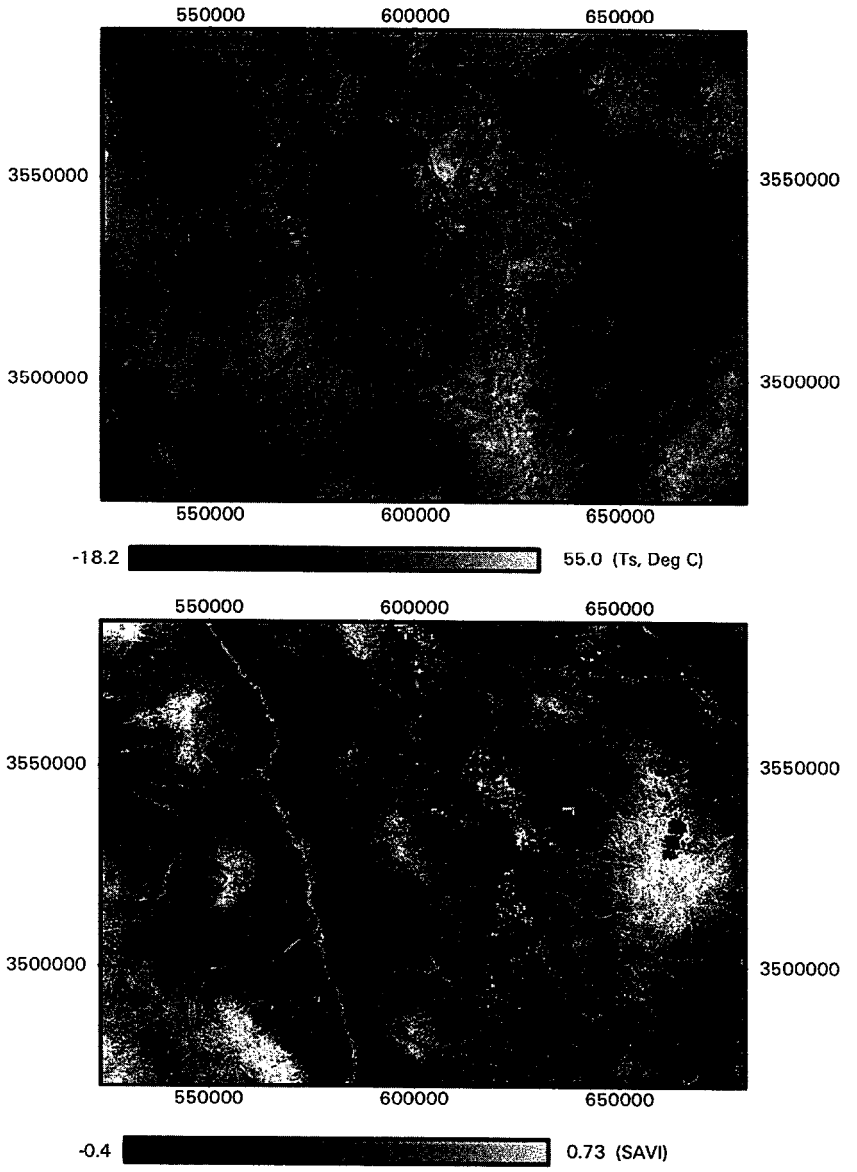

Fig. 2 (continued).

those obtained with the more traditional eddy correlation technique under unstable conditions.

At each MF site and throughout the WG watershed, rainfall was monitored using automated weighing raingages. Weekly cumulative rainfall amounts for Kendall during the WG'92 experiment (Fig. 3(a)) are indicative of the seasonal rainfall pattern in this

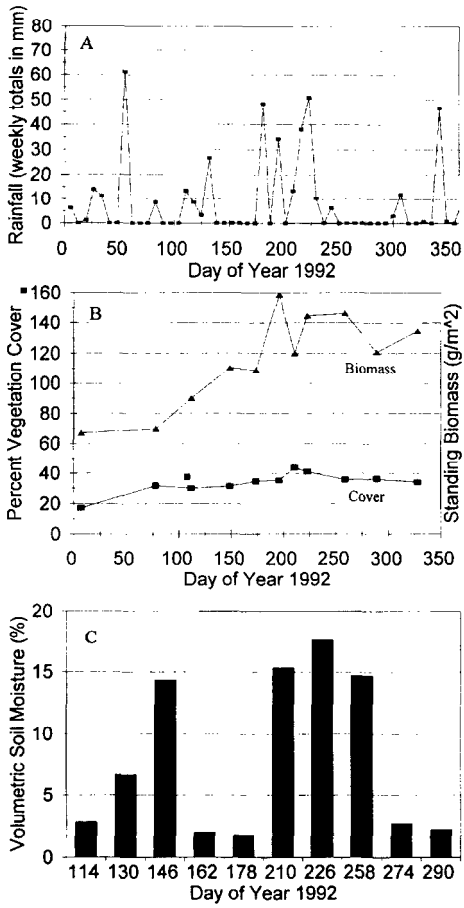

Fig. 3. For the Kendall grassland site during 1992, (a) weekly cumulative rainfall amounts (mm), (b) vegetation biomass ($g m^{-2}$) and cover (%), and (c) volumetric soil moisture (%) to 5 cm depth.

region. That is, annual precipitation is about 300 mm total, with approximately two thirds falling during the 'monsoon' season (July–September). It should be noted, however, that the rainfall during Spring 1992 was greater than normal.

For the regional-scale analysis, maps of T_a and U were created from meteorological data obtained from 13 existing weather stations located throughout the TM scene (Rahman et al., 1994). Hourly air temperature data from the weather stations were interpolated to the satellite overpass time (10:15 am). These values were then normalized to sea surface level using a static lapse rate of temperature (obtained from radiosonde data) to obtain sea level air temperature over the region. A two-dimensional linear interpolation method was then use to grid the temperature over the whole region with a grid size of 120 by 120 m. This was then used to regenerate surface-averaged and topography-adjusted temperatures of the grids (Fig. 2(c)) with the help of digital elevation data (Fig. 2(b)) of the region and the static lapse rate of temperature. Similarly,

wind speed values from the thirteen weather stations were interpolated over the region using the above-mentioned two-dimensional interpolation method (Fig. 2(d)).

4.3. Vegetation and soils

At the Kendall site, monthly measurements of vegetation cover, height and volume by species, total leaf area index (LAI), plant biomass, litter, and plant water content were made throughout the experimental period in grazed and ungrazed sites with both southeast- and northwest-facing slopes. In response to the seasonal rainfall patterns in this region, the vegetation biomass and cover are generally highest during the monsoon season (e.g., Kendall grassland biomass measurements, Fig. 3(b)). Gravimetric soil moisture samples of the upper 5 cm (three replications) were collected at four or five sites within WG, including Kendall, during each Landsat overpass (Fig. 3(c)).

4.4. Atmospheric measurements

Measurements of incident solar illumination were made with a solar radiometer over the time period from sunrise to solar noon and total optical depth of the atmosphere was determined from the slopes of Langley plots (Slater et al., 1987). Total optical depth was partitioned into Rayleigh, aerosol, and ozone optical depths using the procedure described by Biggar et al. (1990). These values were used as input to the Herman–Browning radiative transfer code (RTC) to provide at-satellite radiance values for several assumed values of surface reflectance, ranging from 0.02 to 0.6 (Moran et al., 1992). Based on these RTC-derived values and the Landsat TM sensor calibration, TM digital data were converted to surface reflectance factors. Radiosonde profiles of atmospheric temperature, water content and pressure were also available during each Landsat overpasses at nearby Ft. Huachuca military base. These values were used as input to the Lowtran RTC to allow retrieval of surface temperatures from the Landsat thermal data (Washburne, 1994).

4.5. Remotely sensed spectral data

Ground-based observations of surface reflectance and temperature were made over designated areas at the Kendall site using Exotech [2] 4-band radiometers, a Barnes Modular Multispectral Radiometer (MMR) and Everest infrared thermometers (IRT) during the Landsat overpasses. The ground target covered a large area (480 m by 120 m) over both north- and south-facing slopes representing multiple resolution cells (pixels) of the Landsat TM sensor. Radiometers were mounted in portable yokes at a height of 2 m (resulting in a spatial resolution of about 0.5 m) and deployed over a fine sampling grid resulting in nearly 400 samples over the Kendall target.

[2] The use of company names and brand names are necessary to report factually on available data; however, the authors' affiliations neither guarantee nor warrant the standard of the product, and the use of the name implies no approval of the product to the exclusion of others that may also be suitable.

For a number of overpass dates (Table 1), a Cessna aircraft was flown along two parallel transects intercepting the locations of 8 Metflux sites within WG, with instruments including a 4-band radiometer with Landsat Thematic Mapper (TM) filters (TM1–TM4), an IRT, color video camera and occasionally a thermal-IR scanner. The aircraft flew at a nominal altitude of 100 m above ground level (resulting in a spatial resolution (a pixel) of approximately 25 m diameter on the surface) and flights were scheduled to coincide with the Landsat overpass times (approximately 10:30h).

Eight Landsat TM scenes images were acquired to monitor the seasonal surface changes associated with the dry, monsoon and post-monsoon seasons (Table 1). The nadir-looking Landsat TM sensor has six reflective bands ranging from 0.45 to 2.35 μm with 30 m spatial resolution and one thermal band (10.42–11.66 μm) with a spatial resolution of 120 m. These images were registered and surface reflectance and temperature were retrieved from the digital numbers. We found that the atmospherically-corrected values of TM-derived surface reflectance compared well with ground- and aircraft-based measurements at the Kendall site (Root Mean Squared Error (RMSE) = 0.007). The atmospherically-corrected values of TM-derived surface temperature were close to values measured by ground- and aircraft-based instruments, but were consistently overestimated by 1.5 to 3°C (Washburne, 1994). This point is important because an error of 1°C in surface temperature could result in an error of 50 $W m^{-2}$ in the estimation of $\boldsymbol{LE}$ (Moran et al., 1989). Examples of the T_s and SAVI images for one date in 1992 (Day Of Year (DOY) 162) are included in Fig. 2(e) and (f).

5. Results

The WDI theory was tested at the local scale using ground-based data at Kendall and at the regional scale using Landsat TM data covering the semiarid region located in the southeast corner of Arizona.

5.1. Local results with ground-based measurements at Kendall

As described in a previous section, yoke-based spectral data were acquired over a grid at the Kendall site, bracketing the time of the Landsat overpass. These data were combined with the Metflux measurements of $\boldsymbol{R}_n$, $\boldsymbol{G}$, T_a, U, and VPD to compute WDI for the site on each of 13 days. Unlike the agricultural site for which Moran et al. (1994a) demonstrated the WDI, the Kendall grassland site never reaches full-cover; at a maximum, the vegetation cover is only about 45%. Thus, it becomes difficult to compute the values for points 1 and 2 in Fig. 1. For the agricultural site, Moran et al. (1994a) computed r_a in Eqs. (5) and (6) based on an estimate of surface roughness (z_o) equal to $0.13h$, where h was maximum plant height. For the Kendall site, we computed r_a for points 1 and 2 based on estimates of z_o measured on site during the peak of vegetation biomass in 1990 (Stannard et al., 1994). Then, we computed the VIT trapezoid to extend from SAVI = 0.1 (minimum cover) to SAVI = 0.5 (maximum cover). We computed the VIT trapezoid for each date using this refinement and determined WDI based on an average of the yoke-based measurements of T_s and SAVI on each date.

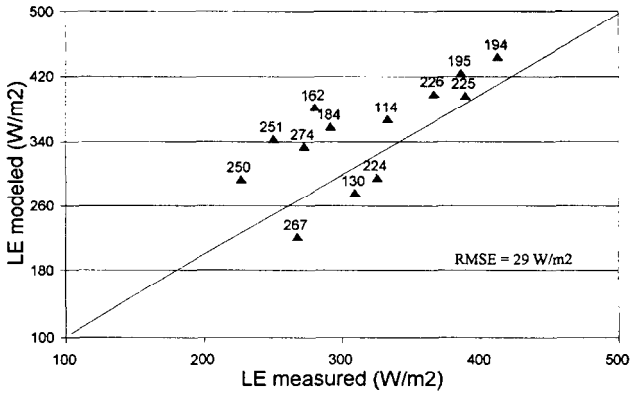

Fig. 4. Comparison of instantaneous actual evapotranspiration ($W m^{-2}$) derived from the WDI model with measurements of evapotranspiration using the Metflux instrumentation. Numbers above symbols represent the day of year 1992.

With a computation of potential $E\Gamma_p$ for each date, we were able to retrieve instantaneous actual $E\Gamma$ (converted to energy units: $W m^{-2}$) [3] from the WDI and compare that with the values of LE measured with Metflux instrumentation (Fig. 4). The 'modeled' values based on the VIT trapezoid compared well with the Metflux values (RMSE = 29 $W m^{-2}$ over a range of LE values from 200–450 $W m^{-2}$), though there was a trend for the modeled LE to overestimate the measured values in most cases (Mean Absolute Difference (MAD) = 45 $W m^{-2}$). This uncertainty was comparable to the uncertainty of conventional ground-based instruments, such as the Bowen ratio and eddy correlation. Kanemasu et al. (1987) reported that LE values could vary by as much as 100% between measurements made with Bowen ratio instruments, and up to 15% with eddy correlation instruments. Kustas et al. (1994) reported that the Metflux measurements of LE were within 20% of those values measured using the eddy correlation technique.

5.2. Regional results with satellite-based measurements

Based on the good results obtained at the local scale, a similar analysis was conducted at the regional scale based on four of the eight Landsat TM scenes acquired during WG'92. The other four images were excluded from this analysis due to variable cloud cover within the scene that could influence the results. The chosen dates were DOYs 162, 178, 274 and 306. DOYs 162 and 178 were just prior to the monsoon season when the vegetation and soil were dry; DOY 274 was post-monsoon season, when the vegetation was more dense but soil conditions were again dry; and on DOY 306, vegetation was mostly senescent (Table 2 and Fig. 3).

[3] The terms $E\Gamma$ and $E\Gamma_p$ are used interchangeably with the terms LE and LE_p, where the former are in units of $mm h^{-1}$ or $mm day^{-1}$ and the latter are expressed in energy units ($W m^{-2}$ or $MJ m^{-2} day^{-1}$).

Table 2
Meteorological and edaphic conditions at Kendall on the dates of the Landsat TM overpasses

DOY 1992	Date	Last rain: date and amount	Amount of rain in last 30 days	Soil Moisture
162	10 June	30 May, 0.5 mm	32 mm	2%
178	26 June	30 May, 0.5 mm	2 mm	2%
274	30 September	20 September, 0.7 mm	7 mm [a]	3%
306	2 November	28 October, 11 mm	14 mm	NA

[a] Rain in August: 117 mm.

Information from the four TM scenes was combined with the interpolated map of T_a to create images of SAVI and $T_s - T_a$. These data were stratified by vegetation biome and plots of SAVI by $T_s - T_a$ were made for each biome. Examples of these are shown for the sage-creosote and alpine biomes and a bare dry playa. The characteristic trapezoidal shape is apparent for the sage-creosote biome (Fig. 5). This would suggest that the vegetation and soil conditions within this biome range from sparse to dense vegetation and from dry to wet soil conditions. However, there are a variety of other variables that could contribute to this scatter, including effects of topography on SAVI

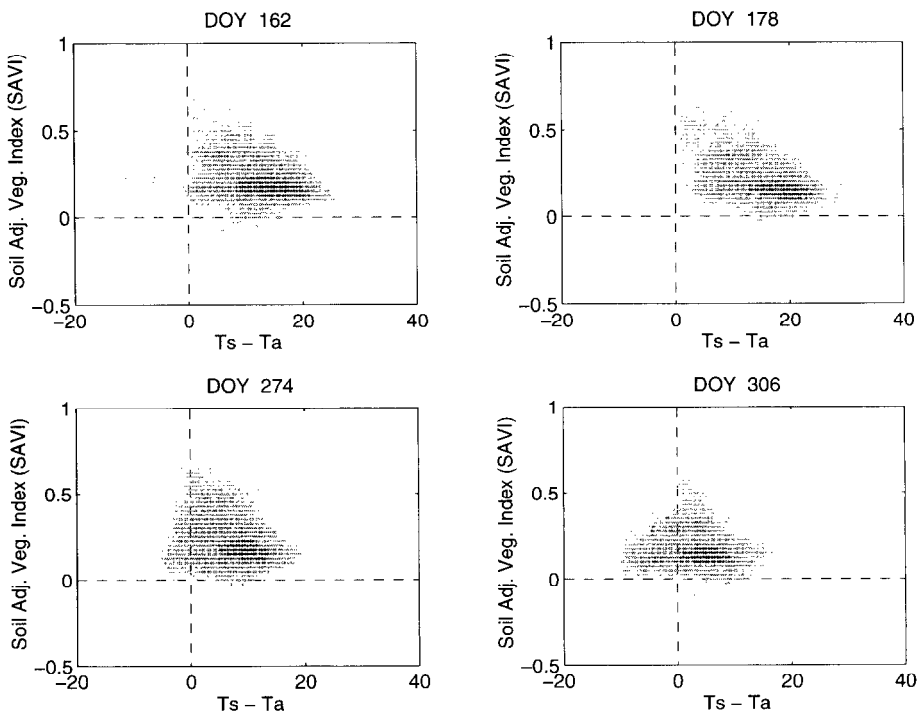

Fig. 5. Scattergram of $(T_s - T_a)$ by SAVI from the four Landsat TM scenes for the sage/creosote biome.

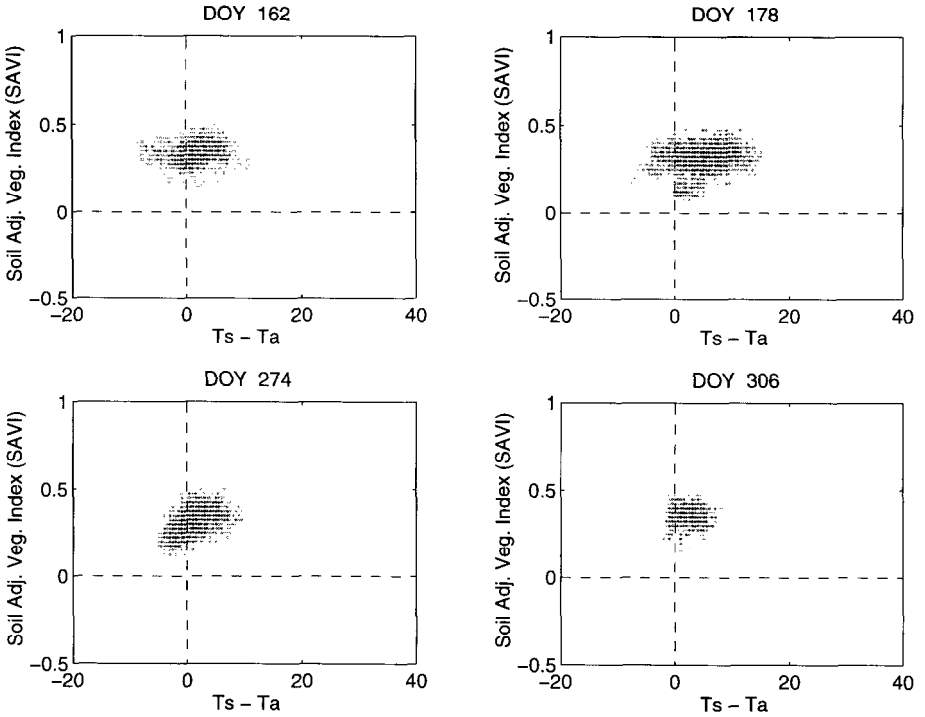

Fig. 6. Scattergram of $(T_s - T_a)$ by SAVI from the four Landsat TM scenes for the alpine biome.

and $T_s - T_a$, inadvertent inclusion of vegetation other than that specified by the labeled biome, and the variability of atmospheric scattering and absorption at varying altitudes.

The scatterplot for the alpine biome (Fig. 6) forms an oval shape rather than a trapezoid. This is due to the near-constant vegetation cover, resulting in consistently high values of SAVI. It is notable, however, that the shape and location of the alpine scatterplot relative to the x-axis $(T_s - T_a)$ vary with date. This is due not only to changes in the evaporative cooling, but also to differences in such meteorological conditions as incoming solar radiation, wind speed and vapor pressure.

The scattergram associated with the barren playa (Fig. 7) could be used as a baseline from which to understand the scattergrams of the other biomes. First, comparison of the SAVI value for each date provides a check on the overall data quality. Since the playa supports only minimal vegetation growth, the SAVI should be very consistent with time. If the SAVI were to vary, it would indicate either a problem with the atmospheric correction of the reflective data or a misregistration of the image. Second, the magnitude and range of the $T_s - T_a$ data provide an indication of the surface water status and variability, respectively. For example, the hottest temperatures were associated with DOY 178 (the day of driest conditions, Table 2) and the greatest range of temperatures was associated with DOY 162 (the day associated with more recent rainfall, and possibly, variable soil moisture). Spatial variability in rainfall is high in this area

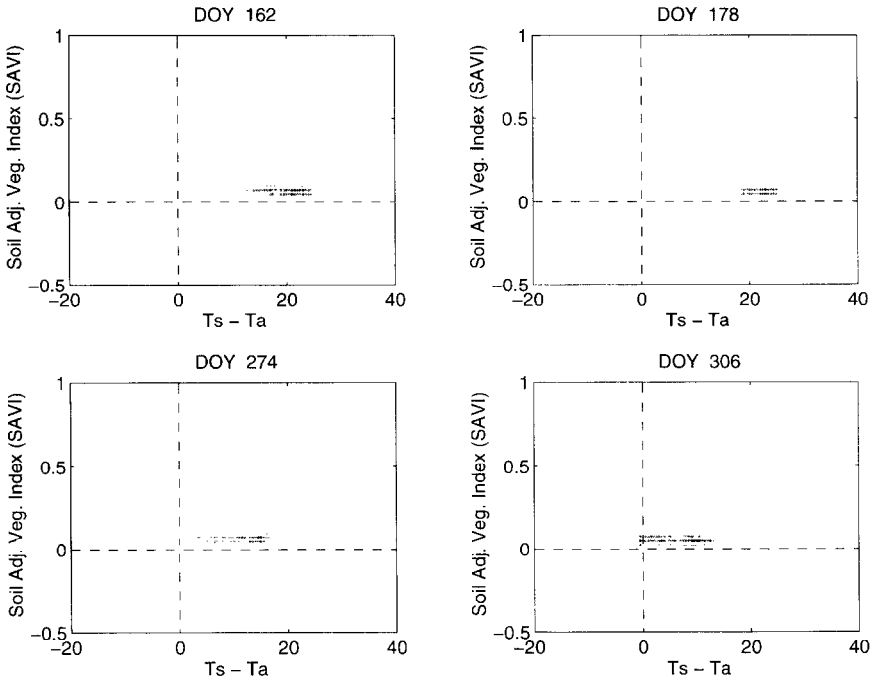

Fig. 7. Scattergram of ($T_s - T_a$) by SAVI from the four Landsat TM scenes for the dry barren playa.

(Renard et al., 1993). Thus, the shape of the data scatter from the barren playa should corroborate the basic knowledge of the vegetation cover, soil moisture status, and meteorological conditions at the site on that day.

Since general information about the grassland biome was known from our local-scale analysis at Kendall, it was possible to compute a trapezoid for this biome for each overpass date. The trapezoid computation was based on the average T_a and U values for the grassland biome derived from the interpolated T_a and U maps. We used values of VPD, R_n and G measured at the Metflux station on each date at Kendall, assuming that these values would be similar for other grasslands in the region at the same general elevation. As with the local-scale analysis, values of surface roughness for points 1 and 2 were based on prior analysis of the grassland biome in 1990 (Stannard et al., 1994) at SAVI = 0.5 (50% vegetation cover). The VIT trapezoids presented in Fig. 8 encompass the data from 0% to 50% vegetation cover and, assuming that the 'warm' and 'cool' edges are linear, can be extended to SAVI = 0.70 (100% vegetation cover).

The VIT trapezoids for the grassland biome (extended to 100% vegetation cover) encompassed the majority of the data on each date (Fig. 8). It is notable that data scatter on DOY 178 (the driest date) did not approach the theoretical 'cool' edge of the trapezoid. On the other three dates, the scatter touched and sometimes exceeded the cool edge. On DOY 162 (the wettest date), the highest density of points was located in the middle of the trapezoid, unlike the other days where the highest density of points was located close to the 'warm edge'.

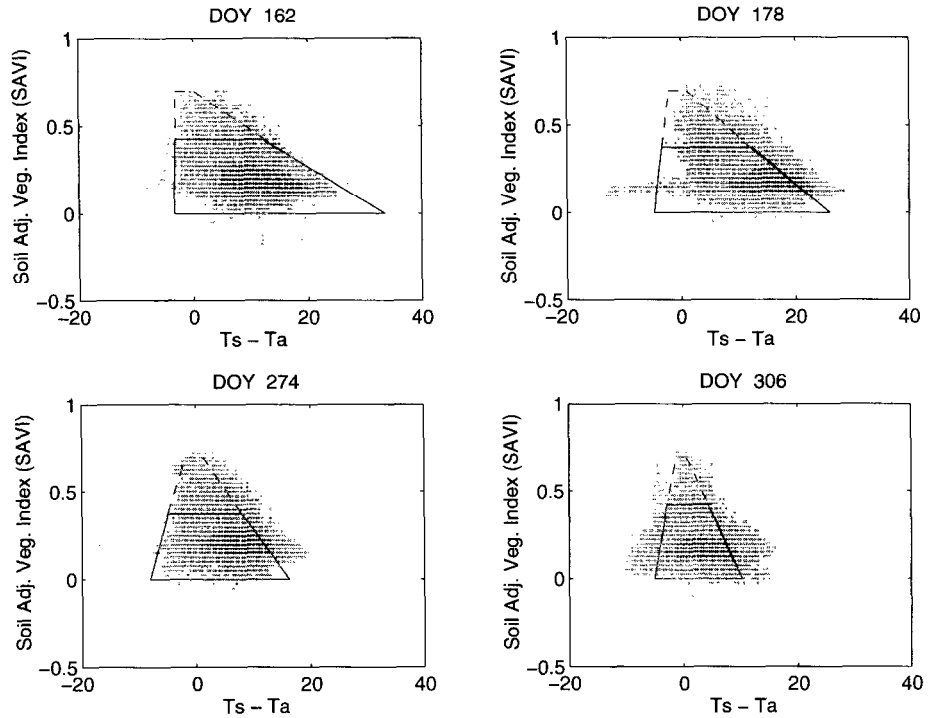

Fig. 8. Scattergram of $(T_s - T_a)$ by SAVI from the four Landsat TM scenes for the grassland biome. The VIT trapezoid was computed for each overpass date based on the average T_a and U values derived from the interpolated T_a and U maps and values of VPD, R_n and G measured at the Metflux station on each date at Kendall. Since surface roughness information was only available for grassland of 50% vegetation cover (SAVI = 0.38), the VIT trapezoid is illustrated here for SAVI values from 0 to 0.38 (solid line). The 'cool' and 'warm' edges could theoretically be extended linearly to SAVI = 0.70 to encompass the data up to 100% vegetation cover (dashed line).

Based on Eq. (13), a computation of potential instantaneous evaporation (LE_p), and the VIT trapezoids from Fig. 8, we were able to compute the actual instantaneous evaporation rate associated with each pixel within the grassland biome in the Landsat TM image. These estimates are presented in the form of a histogram bounded by values of $LE = 0$ and $LE = LE_p$ in Fig. 9 (see also Table 3). For each day, the majority of the LE values were between $LE = 0$ and $LE = LE_p$, though there was a tendency for some estimates of LE to be erroneously less than zero (e.g., DOYs 178, 274 and 306). It appeared that either the VIT trapezoid method tended to underestimate the temperature of the warm edge or the surface temperature data from the Landsat TM images were overestimated. Based on the right-hand side of Eq. (8), it is possible that errors in the computation of the warm edge could be due to errors in the calculation of R_n, G or r_a. However, since the method worked well at the local scale (Fig. 4), it appears that these inputs were reasonable. Another source of error could be the calibration and atmospheric correction of the remotely-sensed data, causing an overestimation of the surface

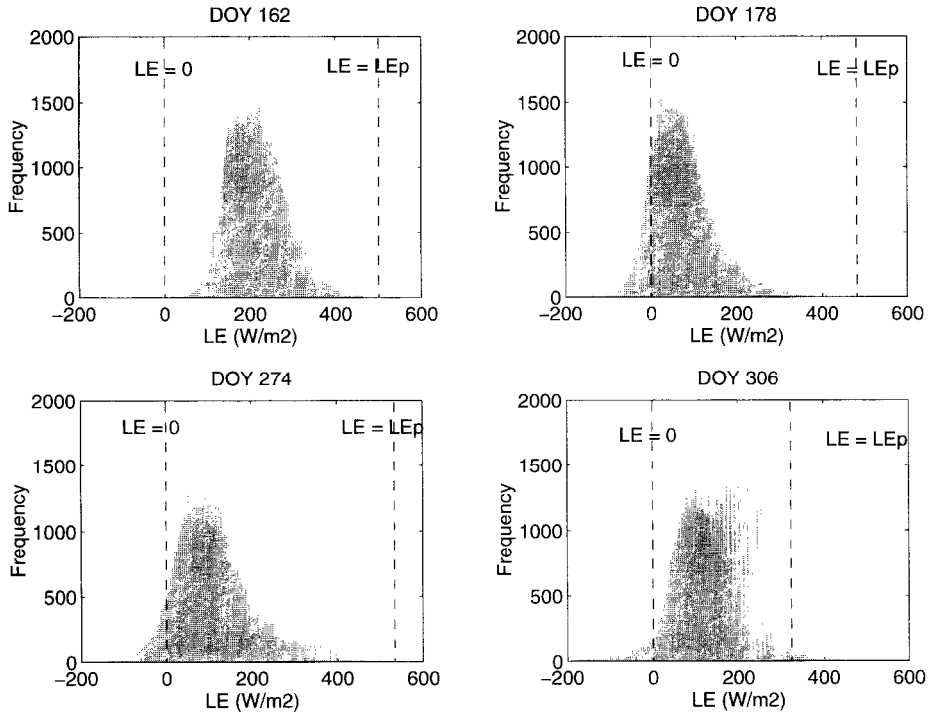

Fig. 9. A frequency histogram of the evaporation rates ($W m^{-2}$) computed using the VIT trapezoid for all pixels within the grassland biome (from Fig. 8). The vertical dashed lines represent the points where ***LE*** equals zero and ***LE*** equals the potential (LE_p). The Water Deficit Index (WDI) was computed from the average of all these data and used to indicate the water status of that biome on each date (Table 3).

temperature. In fact, Washburne (1994) found that the satellite temperatures computed from these 1992 images were consistently warmer (by up to 3°C) than aircraft and ground-based measurements. For the conditions at WG, an error of 1°C in surface temperature could result in an error of 50 $W m^{-2}$ in the estimation of ***LE***. Thus, this 3°C overestimation of surface temperature would account for the majority of the pixels for which ***LE*** was underestimated.

Table 3
Air temperature (T_a), wind speed (U), net radiation (R_n), soil heat flux (G), vapor pressure deficit (VPD), surface temperature (T_s), Soil-Adjusted Vegetation Index (SAVI) and Water Deficit Index (WDI) for the grassland biome at the dates and time (10:30h) of the Landsat TM overpasses

DOY 1992	T_a	U	R_n	G	VPD	T_s	SAVI	WDI
162	25.6	2.0	670	308	3.99	31.3	0.20	0.40
178	23.8	2.8	660	313	4.84	35.0	0.18	0.60
274	23.8	5.3	562	250	3.43	28.8	0.20	0.62
306	16.2	5.0	471	228	1.28	19.6	0.16	0.60

6. Concluding remarks

Based on analysis at the local and regional scale, it appears that this approach is reasonable and has some potential for mapping evaporation rates of heterogeneous landscapes. Assuming that the vegetation type is known (using a biome map or other information), the inputs required were

1. spatially-distributed meteorological measurements of T_a, U, R_n, G, and VPD,
2. remotely sensed measurements of T_s and SAVI, and
3. estimates of z_o, and d_o.

In this analysis, we used measurements of R_n and G at a local grassland site. The approach would be more regionally applicable if the techniques described by Jackson et al. (1985) and Clothier et al. (1986) were used to map R_n and G over heterogeneous areas. Our values of z_o and d_o were taken from measurements at Kendall in 1990. For regional applications, it would be preferable to use reasonable estimates of z_o for general biome types, such as those suggested by Reiners et al. (1994). Future work with the data set presented here will be focused on these two refinements.

The sources of error for application of this approach at the regional scale are numerous and need to be analyzed for impact on the results. A sensitivity analysis will be performed to investigate the effects of topography on surface reflectance and temperature measurements, the error associated with applying an atmospheric correction computed at one altitude to an image composed of multiple altitudes, and the sensitivity of the procedure to differences in surface emissivity. The error associated with variations in emissivity could be reduced by estimating the surface emissivity from measurements of surface reflectance, as suggested by Van de Griend and Owe (1993).

One idea that was mentioned briefly here and deserves further consideration is the use data from a large bare soil site within the image as a baseline from which to understand the scattergrams of the other biomes. This approach would only be applicable to certain scenes but may hold some promise to minimize the meteorological measurements required by the technique.

Acknowledgements

This research was made possible by the cooperative spirit of Steve Land of EOSAT Corp. who provided Landsat TM images at no cost. Support was also provided by the NASA Interdisciplinary Research Program in Earth Sciences (NASA Ref. Num. IDP-88-086), the NASA Eos Program (NASA Ref. Num. NAG-W2425), and NSF (BSC-8920851). We also appreciate the cooperation and assistance of personnel at the USDA ARS Southwest Watershed Research Center, Tucson, and the USDA ARS Tombstone facility.

References

Allen, R.G., 1986. A Penman for all seasons. J. Irrig. Drain. Eng., 112: 348–368.

Biggar, S.F., Gellman, D.I. and Slater, P.N., 1990. Improved evaluation of optical depth components from Langley plot data. Remote Sens. Environ., 32: 91–101.

Carlson, T.N., Perry, E.M. and Schmugge, T.J., 1990. Remote estimation of soil moisture availability and fractional vegetation cover for agricultural fields. Agric. For. Meteorol., 52: 45–69.

Carlson, T.N., Gillies, R.R. and Perry, E.M., 1994. A method to make use of thermal infrared temperature and NDVI measurements to infer surface soil water content and fractional vegetation cover. Remote Sens. Rev., 9: 161–73.

Clothier, B.E., Clawson, K.L., Pinter Jr., P.J., Moran, M.S., Reginato, R.J. and Jackson, R.D., 1986. Estimation of soil heat flux from net radiation during the growth of alfalfa. Agric. For. Meteorol., 37: 319–329.

Friedl, M.A. and Davis, F.W., 1994. Sources of variation in radiometric surface temperature over a tallgrass prairie. Remote Sens. Environ., 48: 1–17.

Gillies, R.R., Cui, J., Carlson, T.N., Kustas, W.P. and Humes, K.S., 1995. Implications of the NDVI and surface radiant temperature relationship. In: Proceedings of the American Meteorological Society Conference on Hydrology, Dallas, TX, January. pp. 157–60.

Goward, S.N. and Hope, A.S., 1989. Evapotranspiration from combined reflected solar and emitted terrestrial radiation: preliminary FIFE results from AVHRR data. Adv. Space Res., 9: 239–249.

Hope, A.S., 1988. Estimation of wheat canopy resistance using combined remotely sensed spectral reflectance and thermal observations. Remote Sens. Environ., 24: 369–383.

Hope, A.S. and McDowell, T.P., 1992. The relationship between surface temperature and a spectral vegetation index of a tallgrass prairie: effects of burning and other landscape controls. Int. J. Remote Sens., 13: 2849–2863.

Huete, A.R., 1988. A soil-adjusted vegetation index (SAVI). Remote Sens. Environ., 27: 47–57.

Huete, A.R. and Jackson, R.D., 1988. Soil and atmosphere influences on the spectra of partial canopies. Remote Sens. Environ., 25: 89–105.

Jackson, R.D., Idso, D.B., Reginato, R.J. and Pinter Jr., P.J., 1981. Canopy temperature as a crop water stress indicator. Water Resour. Res., 17: 1133–1138.

Jackson, R.D., Pinter Jr., P.J. and Reginato, R.J., 1985. Net radiation calculated from remote multispectral and ground station meteorological data. Agric. For. Meteorol., 35: 153–164.

Kanemasu, E.T., Asrar, G., Nie, D., Watts, D., Fritschen, L., Gay, L., Weaver, H., Tanner, B., Tanner, M., Green, J. and Stannard, D., 1987. Inter- and intra-sensor comparisons among Bowen-ratio and eddy correlation instruments. International Symposium On Flow and Transport in the Natural Environment: Advances and Applications, Canberra, Australia, 31 August–4 September.

Kustas, W.P. and Goodrich, D.C., 1994. Preface to the special section on MONSOON'90. Water Resour. Res., 30: 1211–1225.

Kustas, W.P., Blanford, J.H., Stannard, D.I., Daughtry, C.S.T., Nichols, W.D. and Weltz, M.A., 1994. Local energy flux estimates for unstable conditions using variance data in semiarid rangelands. Water Resour. Res., 30: 1351–1361.

Loveland, T.R., Merchant, J.W., Ohlen, D.O. and Brown, J.F., 1991. Development of a land-cover characteristics database for the conterminous US. Photog. Eng. Remote Sens., 57: 1453–1463.

Monteith, J.L., 1973. Principles of Environmental Physics. Edward Arnold, London.

Moran, M.S., Jackson, R.D., Raymond, L.H., Gay, L.W. and Slater, P.N., 1989. Mapping surface energy balance components by combining Landsat Thematic Mapper and ground-based meteorological data. Remote Sens. Environ., 30: 77–87.

Moran, M.S., Jackson, R.D., Slater, P.N. and Teillet, P.M., 1992. Evaluation of simplified procedures for retrieval of land surface reflectance factors from satellite sensor output. Remote Sens. Environ., 41: 169–184.

Moran, M.S., Clarke, T.R., Inoue, Y. and Vidal, A., 1994a. Estimating crop water deficit using the relation between surface-air temperature and spectral vegetation index. Remote Sens. Environ., 49: 246–263.

Moran, M.S., Clarke, T.R., Kustas, W.P., Weltz, M.A. and Amer, S.A., 1994b. Evaluation of hydrologic parameters in semiarid rangeland using remotely sensed spectral data. Water Resour. Res., 30: 1287–1297.

Nemani, R.R. and Running, S.W., 1989. Estimation of regional surface resistance to evapotranspiration from NDVI and thermal-IR AVHRR data, J. Appl. Meteorol., 28: 276–284.

Nemani, R., Pierce, L., Running, S. and Goward, S., 1993. Developing satellite derived estimates of surface moisture status, J. Appl. Meteorol., 32: 548–557.

Price, J.C., 1990. Using spatial context in satellite data to infer regional scale evapotranspiration, IEEE Trans. Geosci. Remote Sens., GE-28: 940–948.

Rahman, A.F., Washburne, J.C., Moran, M.S., Batchily, A.K. and Hodshon-Yates, M., 1994. Mapping surface energy fluxes of a semiarid region in Arizona. In: Proceedings of the IEEE Geoscience and Remote Sensing Symposium, August, Pasadena, CA. pp. 184–186.

Reiners, W.A., Embury, J.B. and Driese, K.L., 1994. Canopy structure and roughness length for Great Plains grassland and intermountain shrublands. In: Proceedings of the AGU Annual Meeting, 4–8 December, San Francisco, CA. EOS, 75: 106.

Renard, K.G., Lane, L.J., Simanton, J.R., Emmerich, W.E., Stone, J.J., Weltz, M.A., Goodrich, D.C. and Yakowitz, D.S., 1993. Agricultural impacts in an arid environment: Walnut Gulch case study. Hydrol. Sci. Tech., 9: 145–190.

Sellers, P.J., 1987. Canopy reflectance, photosynthesis, and transpiration. II. The role of biophysics in the linearity of their interdependence. Remote Sens. Environ., 21: 143–183.

Slater, P.N., Biggar, S.F., Holm, R.G., Jackson, R.D., Mao, Y., Moran, M.S., Palmer, J.M. and Yuan, B., 1987. Reflectance- and radiance-based methods for the in-flight absolute calibration of multispectral sensors. Remote Sens. Environ., 22: 11–37.

Stannard, D.I., Blanford, J.H., Kustas, W.P., Nichols, W.D., Amer, S.A., Schmugge, T.J. and Weltz, M.A., 1994. Interpretation of surface flux measurements in heterogeneous terrain during the Monsoon '90 experiment. Water Resour. Res., 30: 1227–1239.

Van de Griend, A.A. and Owe, M., 1993. On the relationship between thermal emissivity and the normalized difference vegetation index for natural surfaces. Int. J. Remote Sens., 14: 1119–1131.

Washburne, J.C., 1994. A distributed surface temperature and energy balance model of semi-arid watershed. Ph.D. Dissertation, University of Arizona, Department of Hydrology and Water Research. 412 p.